Talanta 223 (2021) 121716

Contents lists available at ScienceDirect

Talanta

journal homepage: www.elsevier.com/locate/talanta

A sensitive biomolecules detection device with catalytic hairpin assembly and cationic conjugated polymer-assisted dual signal amplification strategy

Zhen Zhang [a], Xia Xiang [b,**], Yuqiang Hu [a], Yuhan Deng [a], Longjie Li [a], Wenbo Zhao [c,***], Tongbo Wu [a,*]

[a] School of Pharmacy, Tongji Medical College, Huazhong University of Science and Technology, Wuhan, 430030, China
[b] Oil Crops Research Institute of the Chinese Academy of Agricultural Sciences, Wuhan, 430062, China
[c] State Key Laboratory of NBC Protection for Civilian, Beijing, 102205, China

ARTICLE INFO

Keywords:
Catalytic hairpin assembly
Cationic conjugated polymers
Graphene oxide
Fluorescence resonance energy transfer

ABSTRACT

A simple, sensitive, selective, and enzyme-free homogeneous fluorescent biosensing device for DNA and protein detection is fabricated based on catalytic hairpin assembly (CHA), cationic conjugated polymer (CCP), and graphene oxide (GO). In this biosensing device, CCP together with CHA, provides dual signal amplification, and GO suppresses the background when the target is absent. Thus, this CHA/CCP/GO-based biosensor shows improved sensitivity compared with conventional CHA-based biosensors. In the biosensor, two 6-carboxyfluorescein (FAM)-labeled hairpin DNA probes (H1 and H2) are designed, and in the initial state, they could absorb on the surface of GO, leading the system to produce a low background fluorescence signal. When the target DNA appears, it continually catalyzes the formation of H1–H2 double-stranded DNA (dsDNA) complex by CHA reaction, which could be regarded as the first-step amplification. At the same time, the H1–H2 dsDNA complex departures from the surface of GO and interacts with CCP through electrostatic interaction. Then, CCP provides the second-step amplification due to its high fluorescence resonance energy transfer (FRET) efficiency from CCP to FAM. The limit of detection (LOD) and the limit of quantification (LOQ) for the target DNA could reach 32 pM and 1 nM, respectively. The linear range was from 0.1 to 40 nM, and relative standard deviation (RSD) for the points on the calibration curve ranged from 2.8% to 13.9%. This strategy could also be applied to protein detection potentially by integrating the aptamer of the target protein into the hairpin DNA. As proof of concept, thrombin was detected, and the LOD and LOQ was 11 pM and 33 pM, respectively. The linear range was from 3 to 54 nM, and RSD ranged from 3.3% to 10.4%. It showed good selectivity for thrombin compared to equal concentrations of interferences. It was also applied to quantify the thrombin (5, 10, 20 nM) in 1% spiked human serum, which showed satisfying recovery in the range of 94.7 ± 5.3 to 103.7 ± 4.9%.

1. Introduction

Simple, sensitive, and selective detection of DNA and protein are both of high demand in the field of medical diagnostics, forensic investigation, food safety and environmental science [1,2]. Unfortunately, the content of related analytes in natural environments is relatively low, which poses a considerable challenge to detection [3]. Various amplification strategies have been developed to overcome this problem, such as polymerase chain reaction (PCR) [4], loop-mediated isothermal amplification (LAMP) [5], ligase chain reaction (LCR) [6], rolling circle amplification (RCA) [7] and endonuclease or exonuclease assisted amplification [8,9]. However, in these strategies, high sensitivity is relying on the use of one or multiple enzymes. The enzymes significantly increase system cost and complexity and limit the universal application of the strategies. Recently, catalytic hairpin assembly (CHA), which achieves signal amplification just through the target hybridization, is proposed as a promising enzyme-free signal amplification tool [10–12]. Though the enzyme is needless in the CHA amplification assay, the detection sensitivity is unsatisfactory. For example, Li et al. constructed a CHA-based fluorescent biosensor for DNA detection, and the

* Corresponding author.
** Corresponding author.
*** Corresponding author.
E-mail addresses: xiangshi19850130@163.com (X. Xiang), zhaowb1987@126.com (W. Zhao), wutongbo@hust.edu.cn (T. Wu).

https://doi.org/10.1016/j.talanta.2020.121716
Received 5 August 2020; Received in revised form 16 September 2020; Accepted 28 September 2020
Available online 30 September 2020

detection limit of 0.2 nM was obtained [13]. To further enhance the sensitivity of CHA, multiple CHA synergetic reactions [14], CHA/DNAzyme-based amplification [15], CHA/enzyme-assisted circulation [16] or CHA/nanomaterials-conjugated magnified strategy was developed in CHA-based detection system [17]. However, the majority of these strategies are time-consuming and need complicated and precious designs to generate the analytical signal. For example, Ye et al. developed a fluorescent DNA sensor by the formation of CHA-induced branched DNA structure and the in-suit synthesis of copper nanoparticles (CuNPs). The detection limit for the target DNA reached 44 pM [18]. In this assay, Exo III was introduced to reduce the background signal, which discarded the enzyme-free intrinsic property of CHA. On the other hand, the signal producing process needed to add Cu^{2+} and ascorbate, which increased the complexity of this system. Thus, a simple, sensitive, robust and enzyme-free biomolecular detection strategy is still in need.

Cationic conjugated polymers (CCPs) have been promising materials for bioanalysis due to their excellent optical properties and capabilities [19,20]. The polymers can easily bind with single- or double-stranded nucleic acids with electrostatic interactions [21–23]. As an energy donor, CCP can transfer the high energy to the acceptor through fluorescence resonance energy transfer (FRET) and enhance the fluorescence emission intensity of the acceptor [24]. So CCP can be directly used to combine with the product complex of CHA (commonly double-stranded DNA, dsDNA) and produce an amplified signal for the energy acceptor (such as the fluorophore) on the dsDNA. As CCP could also bind with the hairpin DNA, the background signal without the target will affect the detection performance. To solve this problem, we proposed to introduce graphene oxide (GO) into the reaction system. GO, as a single-layer two-dimensional carbon nanomaterial, has received great attention owing to its unique characteristics, including superior and universal fluorescence quenching property and different absorption ability toward nucleic acids with different structures [25,26]. With the aid of these properties, GO-based sensors have been successfully built to detect different biomolecular targets [27,28]. For instance, Huang et al. developed a graphene oxide-based thrombin detection assay with a limit detection of 22.8 pM [29]. In this strategy, the high sensitivity was achieved by coupling polymerase induced thrombin cycling and nicking enzyme assisted signal amplification. However, multiple enzymes and operating steps were involved.

Herein, we designed a simple, enzyme-free, dual amplified biosensor device for sensitive biomolecules detection by taking advantages of CHA, CCP, and GO and minimizing the shortcomings of them. The first amplification relied on the recycling of target molecular in the CHA reaction. Then, poly (9,9-bis(6′-N, N, N-trimethylammonium)hexyl)-fluorenylene phenylene dibromide (PFP), as one kind of CCPs, was introduced into the system. PFP could enhance the fluorescence signal of the fluorophore through the high efficiency FRET process from PFP to the fluorophore and provide the second amplification. GO was used to lower the background signal of the whole system. This strategy has been successfully applied for DNA and protein detections.

2. Materials and methods

2.1. Reagents and instruments

Graphene oxide was purchased from Xfnano Materials Technology Co., Ltd. (Nanjing, China). The oligonucleotides were synthesized and purified with HPLC by Sangon Biotech. Co., Ltd. (Shanghai, China). The sequences of the oligonucleotides used in this work are shown in Supporting Information Table S1. Thrombin, IgG, trypsin, pepsin, papain, BSA, β-dextranase, mucoprotein and lecithin were obtained from Sigma (St. Louis, USA). PFP was synthesized based on the reported method [30]. Fluorescence spectra were recorded by the Hitachi F-7000 fluorescence spectrophotometer (Tokyo, Japan). The excitation and emission slits were both set at 10 nm. Bio-Rad gel-imaging system (California, USA) was used to image the gel electrophoresis picture.

The stock solution of GO stored at room temperature according to the manufacturer recommendation. The prepared solution of oligonucleotides, PFP and the reaction buffer (10 mM Tris, 150 mM NaCl, pH 8.0 for the target DNA detection; 10 mM Tris, 150 mM NaCl, 5 mM $MgCl_2$, pH 8.0 for the thrombin detection) all stored at 4 °C for the further use.

2.2. Optimization of the GO concentration for the target DNA detection

H1 (5 nM), H2 (5 nM), and different concentrations of GO (0, 0.67, 2.00, 4.00, 6.00, 8.00, 10.0, or 12.0 μg mL^{-1}) were mixed into the reaction buffer (10 mM Tris, 150 mM NaCl, pH 8.0) with a 300 μL total volume. After incubation for 10 min at room temperature, the solution was measured by fluorescence spectrophotometer with an excitation wavelength at 480 nm and emission wavelength from 500 to 700 nm.

2.3. Optimization of the reaction time for the target DNA detection

5 nM H1, 5 nM H2, 5 nM target DNA and 4.0 μg mL^{-1} GO were mixed into the reaction buffer (10 mM Tris, 150 mM NaCl, pH 8.0) with a 300 μL total volume. After different incubation time (0, 30, 60, 80, 120, 140 min) at 37 °C, the above solution was measured by fluorescence spectrophotometer with an excitation wavelength at 480 nm and emission wavelength from 500 to 700 nm.

2.4. Optimization of the PFP concentration for the target DNA detection

100 μL reaction buffer (10 mM Tris, 150 mM NaCl, pH 8.0) containing 5 nM H1, 5 nM H2, and 4.0 μg mL^{-1} GO (without the target DNA) or 100 μL reaction buffer containing 5 nM H1, 5 nM H2, 50 nM target DNA and 4.0 μg mL^{-1} GO (with target DNA) were incubated at 37 °C for 2 h. Then different concentrations of PFP (0, 0.27, 0.53, 0.80, 1.07, 1.33, 2.00, 2.67 μg mL^{-1}) and a certain amount of reaction buffer were added for an extra 20 min incubation with a 300 μL total volume. Subsequently, the fluorescence intensity was recorded with an excitation wavelength at 370 nm and emission wavelength from 390 to 700 nm.

2.5. The target DNA detection assay

The target DNA with different concentrations were mixed into 100 μL reaction buffer (10 mM Tris, 150 mM NaCl, pH 8.0) containing 5 nM H1, 5 nM H2 and 4.0 μg mL^{-1} GO. After a 2 h incubation at 37 °C 15 μL PFP (0.04 mg mL^{-1}) and 185 μL reaction buffer were added for an extra 20 min incubation with a 300 μL total volume. Subsequently, the fluorescence intensity was recorded with an excitation wavelength at 370 nm and emission wavelength from 390 to 700 nm.

2.6. Agarose gel electrophoresis

3% agarose gels electrophoresis analysis was performed to validate the occurrence of CHA. The sample under different conditions was mixed evenly with SYBR Green I and 1x bromophenol blue. The electrophoresis was performed in 1x TAE buffer at a constant potential of 100 V for 40 min at room temperature. Then agarose gel electrophoresis picture was obtained by Bio-Rad imaging system (Bio-Rad Laboratories Inc. USA).

2.7. The thrombin detection assay

The thrombin with different concentrations (3.0, 4.8, 6.0, 12, 18, 24, 30, 36, 42, 48, 54 nM) were added in 100 μL reaction buffer (10 mM Tris, 150 mM NaCl, 5 mM $MgCl_2$, pH 8.0) containing 5 nM HT1, 5 nM HT2 and 1.33 μg mL^{-1} GO. After a 2 h incubation at 37 °C, 10 μL PFP (0.04 mg mL^{-1}) and 190 μL reaction buffer were added for an extra 20 min incubation. Subsequently, the fluorescence intensity was recorded with an excitation wavelength at 370 nm and emission wavelength from 390

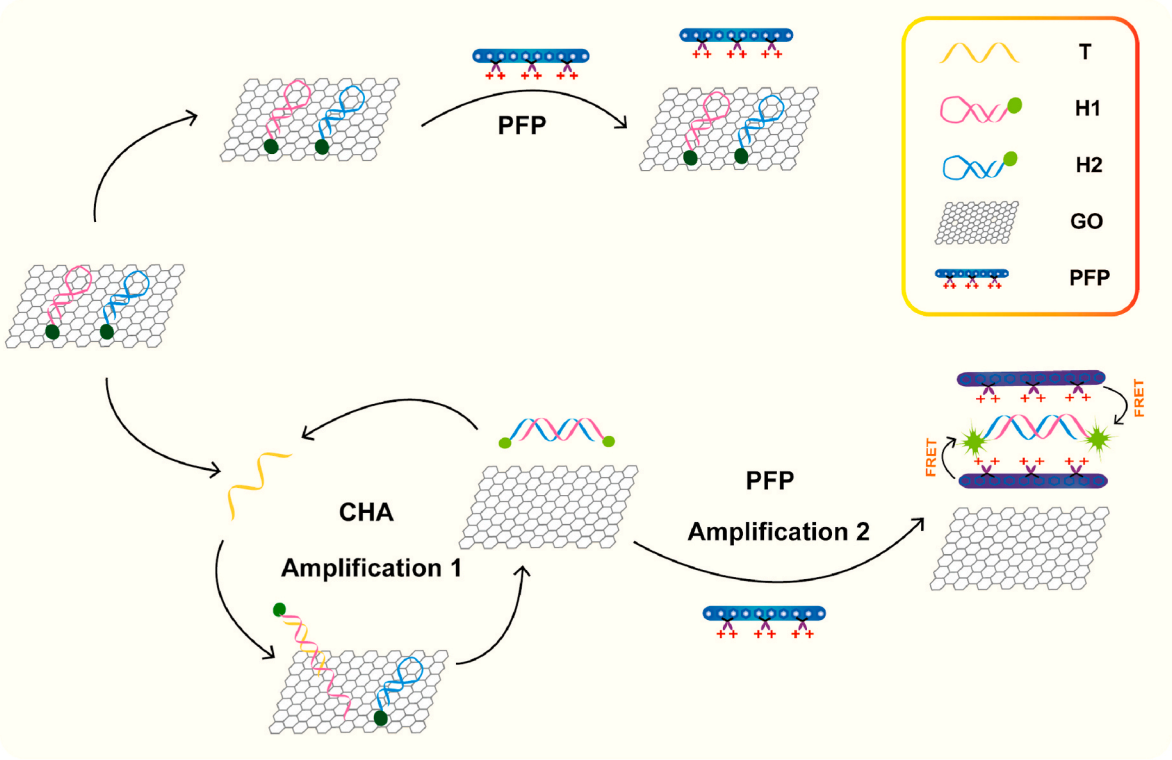

Scheme 1. Schematic illustration of the dual amplification strategy for DNA detection.

to 700 nm.

2.8. Interference testing for the thrombin detection

Several other interferents (IgG, trypsin, pepsin, BSA, β-dextranase, mucoprotein and lecithin) were selected to explore the selectivity of this strategy for thrombin detection. 30 nM thrombin and equal concentrations of above interferents were added into 100 μL reaction buffer (10 mM Tris, 150 mM NaCl, 5 mM $MgCl_2$, pH 8.0) containing 5 nM HT1, 5 nM HT2 and 1.33 μg mL^{-1} GO. After a 2 h incubation at 37 °C, 10 μL PFP (0.04 mg mL^{-1}) and 190 μL reaction buffer were added for an extra 20 min incubation. Subsequently, the fluorescence intensity was recorded with an excitation wavelength at 370 nm and emission wavelength from 390 to 700 nm.

2.9. Thrombin recovery assay in human serum

1% human serum was used in the recovery experiment. Firstly, the human serum was diluted to 1% by the reaction buffer without other special preparation process. Then, thrombin with different concentrations was added to the 1% serum solution. Finally, HT1, HT2, GO, and PFP were added orderly to the above solution according to the procedures for thrombin detection.

2.10. Statistical treatment

Unless otherwise specified, all the samples were repeated three times and the error bars were caculatd as the standard deviation of three independent experiments (n = 3). GraphPad Prism 7 was used to analysis the original data.

3. Results and discussions

3.1. Dual amplification strategy design for DNA detection

Scheme 1 depicts the fluorescent detection principle for the target DNA with a dual amplification strategy. Hairpin probe DNA H1 and H2 are both single-labeled with the fluorophore 6-carboxyfluorescein (FAM) at 5′-terminus. FAM is chosen as the energy acceptor because the fluorescence absorption spectrum of FAM overlaps with the fluorescence emission spectrum of PFP, as shown in Fig. S1, which is consistent with other references [24,31]. Without the target DNA (T), H1 and H2 remain to be hairpin structure. After adding PFP, most of H1 and H2 still tend to adsorb to the surface of GO rather than PFP. As shown in Fig. S2, the background signal of H1-H2-PFP at 525 nm (which is the peak emission wavelength of the FAM after FRET with PFP) with GO was extensively smaller (682 a. u.) than that without GO (1616 a. u.), showing the background suppression effect of GO in the FRET system. While, with the existence of the target DNA, hairpin DNA H1 could be opened by the target DNA and form an exposed terminal sequence, which could hybrid and open the stem-loop structure of H2. Thus, the target DNA will release from H1 through the toehold-mediated DNA strand displacement reaction, and an H1–H2 complex with the dsDNA feature will form. The target DNA could continually react with another H1, and one target DNA strand can induce numerous H1–H2 complexes in the CHA reaction, which could be regarded as the first-step amplification. The H1–H2 complex will depart from the surface of GO due to the weak interaction between GO and rigid dsDNA. PFP will bind with the H1–H2 complex through electrostatic interaction. A high-efficiency FRET from PFP to H1–H2 complex will occur and provide the second-step amplification due to the superior light harvesting ability of PFP. Another advantage of PFP in this system is that it overcomes the problem that dsDNA is hard to bind with other materials, such as CeO_2 [32], gold nanoparticles [33] and MoS_2 [34]. Therefore, the target DNA can be detected with a homogeneous dual amplification strategy by simply monitoring the change of fluorescence intensity at 525 nm with

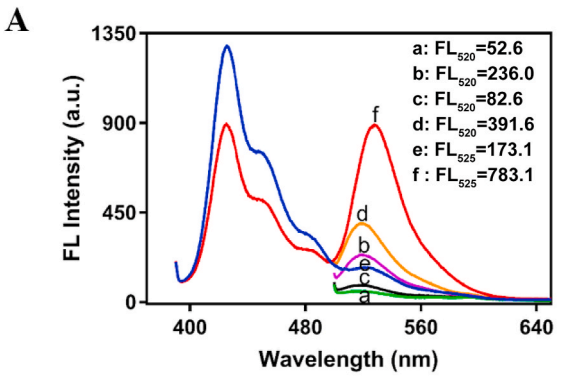

	Curve a	Curve b	Curve c	Curve d	Curve e	Curve f
T		√		√		√
H1	√	√	√	√	√	√
H2			√	√	√	√
GO	√	√	√	√	√	√
PFP					√	√

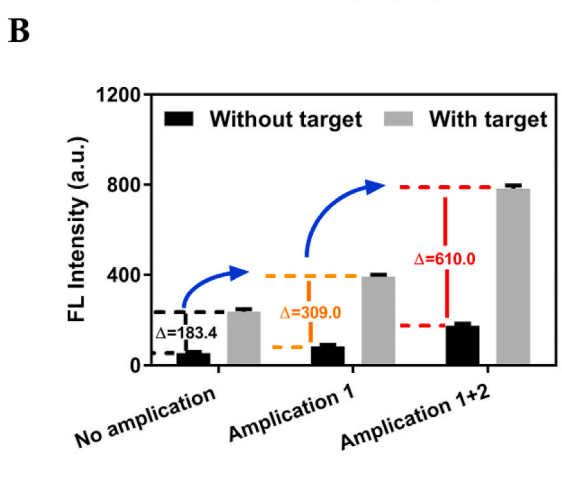

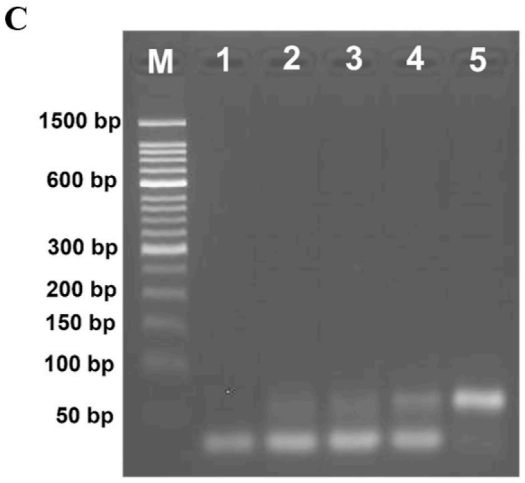

Fig. 1. (A) Fluorescence emission spectra of the system under different conditions and the table of reagents added for each reaction. Curve a: H1+GO; Curve b: H1+T+GO; Curve c: H1+H2+GO; Curve d: H1+H2+T+GO; Curve e: H1+H2+GO+PFP; Curve f: H1+H2+T+GO+PFP. The concentrations of H1, H2, target DNA, GO and PFP were 5 nM, 5 nM, 20 nM, 4 μg mL^{-1} and 2 μg mL^{-1}, respectively. The excitation wavelength was set at 480 nm without PFP and 370 nm with PFP in the reaction system. (B) Histogram of the change of fluorescence intensity with or without target under different conditions. The fluorescence intensities were recorded at 520 nm for No amplification based on the curve a and b in Fig. 1A and Amplification 1 based on the curve c and d in Fig. 1A. The fluorescence intensities were recorded at 525 nm for Amplification 1 + 2 based on the curve e and f in Fig. 1A. Error bars represent the standard deviation of three measurements. (C) Gel electrophoretic analysis of different components in CHA. Lane M: DNA ladder; lane 1: H1; lane 1: H1+H2; lane 3: H1+H2+50 nM T; lane 4: H1+H2+200 nM T; lane 5: H1+H2+500 nM T. The concentrations of H1 and H2 were 500 nM, respectively.

an excitation wavelength at 370 nm.

Firstly, the feasibility of the dual amplification strategy was studied. As shown in Fig. 1A, without amplification, the fluorescence signal of H1 at 520 nm (52.6 a. u.) was strongly quenched by GO (curve a in Fig. 1A, ex: 480 nm). While upon the appearance of the target DNA, H1 hybridized with the target DNA to form T-H1 dsDNA with a sticky end. Thus the T-H1 dsDNA could partially dissociate from the GO surface as a result of little fluorescence recovery at 520 nm (236 a. u.) (curve b in Fig. 1A, ex: 480 nm). The fluorescence recovery at 520 nm was about 183.4 a. u. (No amplification in Fig. 1B). With the aid of CHA amplification (Amplification 1 in Fig. 1B), the fluorescence recovery at 520 nm was about 309.0 a. u. calculated based on curve c and d in Fig. 1A (ex: 480 nm). The fluorescence recovery with CHA increased about 68.5 ± 3.2% compared with that with no amplification, indicating that the target DNA successfully catalyzed hairpin DNA H1 and H2 assembling into dsDNA.

3% agarose gel electrophoresis experiment also verified the successful occurrence of the CHA reaction (Fig. 1C). Fig. 1C clearly showed that there was almost no H1–H2 complex when H1 mixed with H2 directly (lane 2), indicating that the hairpin structure of H1 and H2 are relatively stable in this system. While, in the presence of the target DNA, the band of H1 and H2 (below the 50 bp marker) became dimmer. And a new band corresponding to the H1–H2 complex formed (the band above the 50 bp marker in lane 3, lane 4 and lane 5). With more target DNA, the band of H1–H2 complex became lighter (from lane 3 to lane 5). When FRET occurs from PFP to FAM, the peak of the fluorescence emission spectrum changes from 520 nm to 525 nm [30]. Thus, for the dual amplification, significant fluorescence enhancement at 525 nm was recorded when PFP was added to the reaction mixture above. With the aid of CHA and PFP amplification (Amplification 1 + 2 in Fig. 1B), the fluorescence recovery at 525 nm was about 610.0 a. u. calculated based on curve e and f in Fig. 1A (ex: 370 nm). The fluorescence recovery with the dual signal amplification increased about 233 ± 4.7% compared with that with no amplification.

3.2. *Optimization of the dual amplification strategy for DNA detection*

Then, the concentrations of GO and PFP and the reaction time of CHA were optimized in this system. GO plays an essential role in the whole reaction system. The lack of enough GO will increase the background signal, while the redundant GO will suppress the target signal. As shown in Fig. S3A, different concentrations of GO were added to the system to quench the fluorescence signal of hairpin DNA H1 and H2 without the target DNA. The increasing concentration of GO led to the fluorescence intensity of H1 and H2 decreased obviously. The fluorescence intensity of H1 and H2 reached the platform when the concentration of GO reached 4 μg mL^{-1}. Thus, 4 μg mL^{-1} GO was chosen for further experiments. As reaction time is an important parameter for the CHA reaction, it was also optimized, and the result was shown in Fig. S3B. The result indicated that the CHA reaction could reach equilibrium in 2 h. PFP, as a signal amplifier, also affects the performance of this strategy. We optimized the concentration of PFP under the condition with or without the

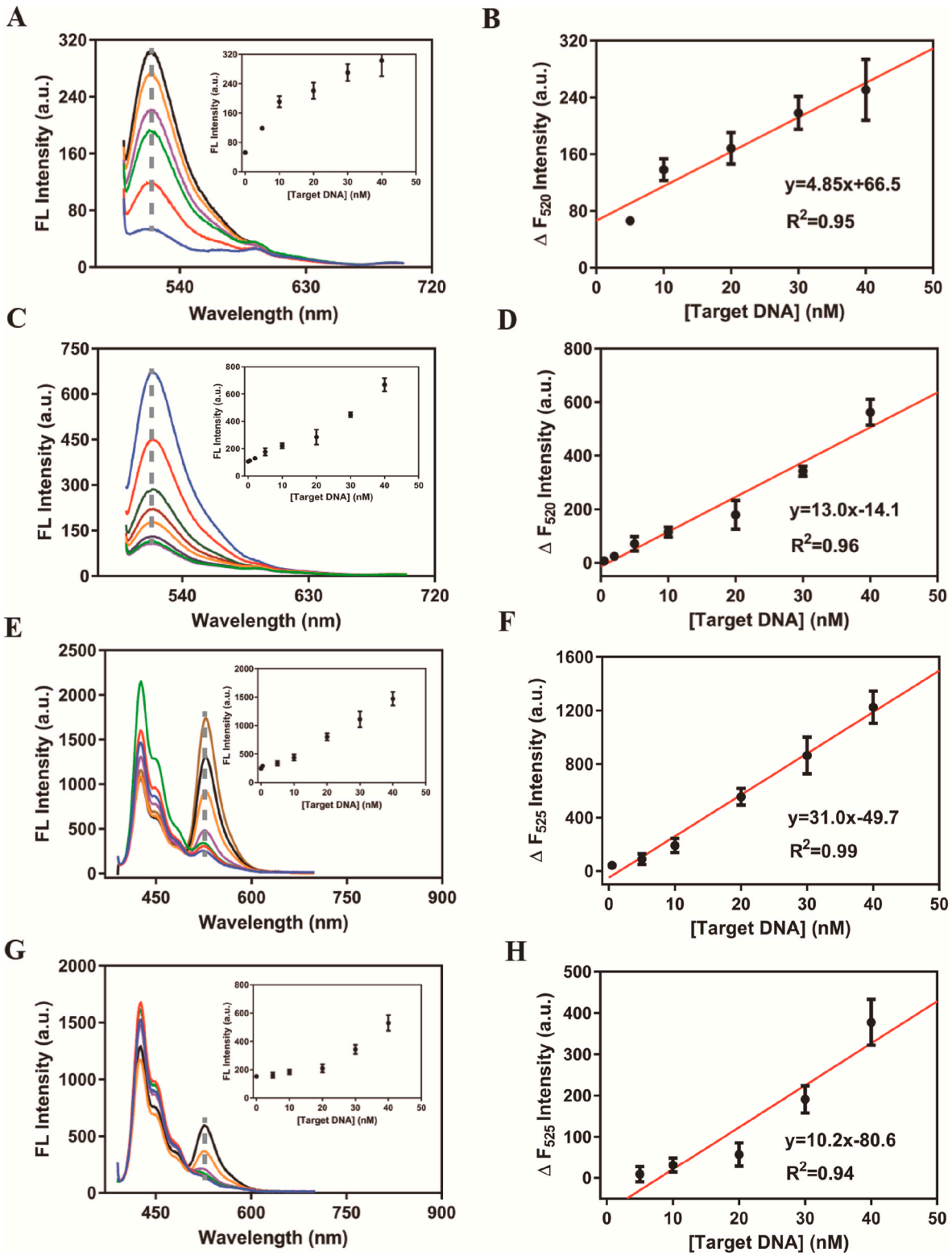

Fig. 2. (A) Fluorescence responses to different concentrations of target DNA (0, 5, 10, 20, 30, 40 nM) using no amplification strategy. The grey dash line shows the peak of FAM signal at 520 nm. The insert shows the fluorescence intensity at 520 nm for different target DNA concentrations. (B) The linear fitting curve of ΔF_{520} and the target DNA concentration using no amplification strategy. (C) Fluorescence responses to different concentrations of target DNA (0, 0.5, 2, 5, 10, 20, 30, 40 nM) with CHA amplification. The grey dash line shows the peak of FAM signal at 520 nm. The insert shows the fluorescence intensity at 520 nm for different target DNA concentrations. (D) The linear fitting curve of ΔF_{520} and the target DNA concentration with CHA amplification. (E) Fluorescence responses to different concentrations of target DNA (0, 0.1, 0.5, 5, 10, 20, 40 nM) with CHA and PFP dual amplification. The grey dash line shows the peak of FAM signal at 525 nm. The insert shows the fluorescence intensity at 525 nm for different target DNA concentrations. (F) The linear fitting curve of ΔF_{525} and the target DNA concentration with CHA and PFP dual amplification. (G) Fluorescence responses to different concentrations of target DNA (0, 5, 10, 20, 30, 40 nM) with PFP amplification. The grey dash line shows the peak of FAM signal at 525 nm. The insert shows the fluorescence intensity at 525 nm for different target DNA concentrations. (H) The linear fitting curve of ΔF_{525} and the target DNA concentration with PFP amplification. Error bars represent the standard deviation of three measurements.

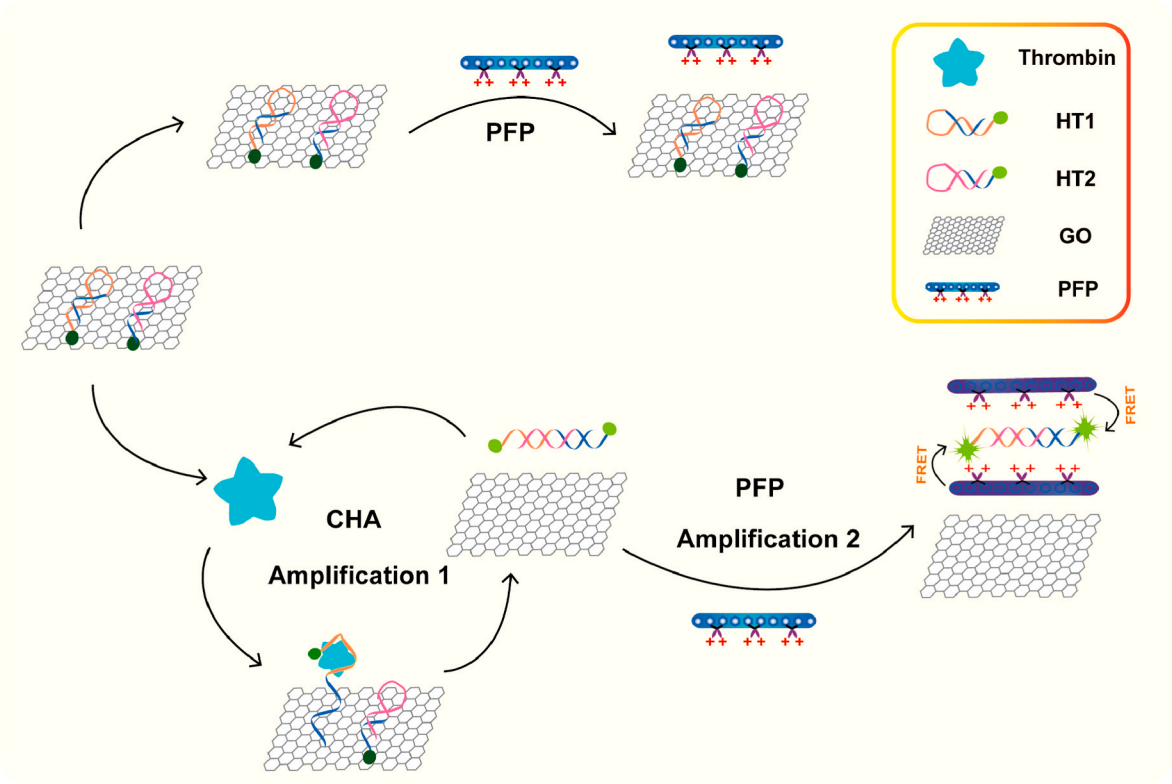

Scheme 2. Schematic illustration of the dual amplification strategy for thrombin detection.

target DNA. As shown in Fig. S3C, with the increasing of PFP concentration, both the fluorescence intensity of the background (without the target DNA) and the signal (with the target DNA) raised at 525 nm with a 370 nm excitation wavelength. When the concentration of PFP was above 2 μg mL^{-1}, the fluorescence intensity of the signal reached the platform, while that of the background still increased. So the concentration of PFP was set as 2 μg mL^{-1} to obtain the largest fluorescence intensity difference between signal and background.

3.3. Sensitivity and selectivity of the dual amplification strategy for DNA detection

Under the optimal experimental condition, the sensitivity for target DNA detection with different detection modes was investigated. Fig. 2A showed the fluorescence spectra with varying concentrations of the target DNA using the strategy of no amplification with excitation wavelength at 480 nm. The insert of Fig. 2A depicted the corresponding fluorescence intensity at 520 nm. Fig. 2B showed the relationship between ΔF_{520} (the fluorescence intensity at 520 nm of the signal minuses that of the background) and the target DNA concentration. And it exhibited an linear response between ΔF_{520} and the target DNA concentration from 5 nM to 40 nM. The regression equation was fitted as $y = 4.85x+66.5$ ($R^2 = 0.95$, the relative standard deviation (RSD) ranged from 8.6% to 17.1%), where y represents the net signal ΔF_{520}, and x is the concentration of the target DNA. The limit of detection (LOD) with this mode was 0.62 nM based on the calculation method of $3\sigma/k$ (where σ represents the standard deviation of the background signal of this reaction system, and k is the slope of the fitted regression equation in the calibration graph, n = 10). And the limit of quantification (LOQ) was calculated as 2.1 nM according to the equation $LOQ = 10\sigma/k$ [35].

Fig. 2C and E showed the fluorescence spectra with different target DNA concentrations by using CHA single amplification (Amplification 1 in Fig. 1B) or CHA and PFP dual amplification (Amplification 1 + 2 in Fig. 1B) detection mode, respectively. With CHA amplification alone (ex: 480 nm and em: 520 nm), the corresponding fitted regression equation was $y = 13.0x-14.1$ ($R^2 = 0.96$, RSD ranged from 5.4% to 16.5%) with the LOD and LOQ to be 0.23 nM and 0.77 nM, respectively (Fig. 2D). With CHA and PFP dual amplification (ex: 370 nm and em: 525 nm), the corresponding fitted regression equation was $y = 31.0x-49.7$ ($R^2 = 0.99$, RSD ranged from 2.8% to 13.9%) with the LOD and LOQ to be 32 pM and 0.1 nM (Fig. 2F).

We also detected the target DNA only using PFP amplification by adding target, H1, GO, and PFP into the reaction system (ex: 370 nm and em: 525 nm) (Fig. 2G). The corresponding fitted regression equation was $y = 10.2x-80.6$ ($R^2 = 0.94$, RSD ranged from 4.7% to 17.3%) with the LOD and LOQ to be 0.10 nM and 0.33 nM (Fig. 2H), which is better than that with no amplification.

Compared with other enzyme-free DNA detection methods, this simple dual amplification provided better or comparable sensitivity (Table S2). The selectivity of our dual amplification method was also tested. As shown in Fig. S4, the perfectly matched target DNA induced a remarkable fluorescence recovery, while the fluorescence recovery with single-base mismatched DNA was only 50% of that with the perfectly matched target DNA. Two-base mismatched or random sequence DNA produced little fluorescence recovery. The results indicated that our method has the single-base level specificity.

3.4. Dual amplification strategy for the thrombin detection

Next, we tried to apply our dual amplification strategy to protein detection and chose thrombin as the target to validate the proof of concept. Thrombin, as a proteolytic enzyme, can catalyze the conversion of fibrinogen into fibrin to promote blood coagulation, which is of great significance for the diagnosis and treatment of related diseases [36]. Besides, the binding aptamers of thrombin have been selected in vitro as early as 1997 [37]. Subsequently, thrombin is often used as a model for quantitative protein detection in aptamer-based biosensors [38].

As shown in Scheme 2, hairpin DNA HT1 and HT2 were designed.

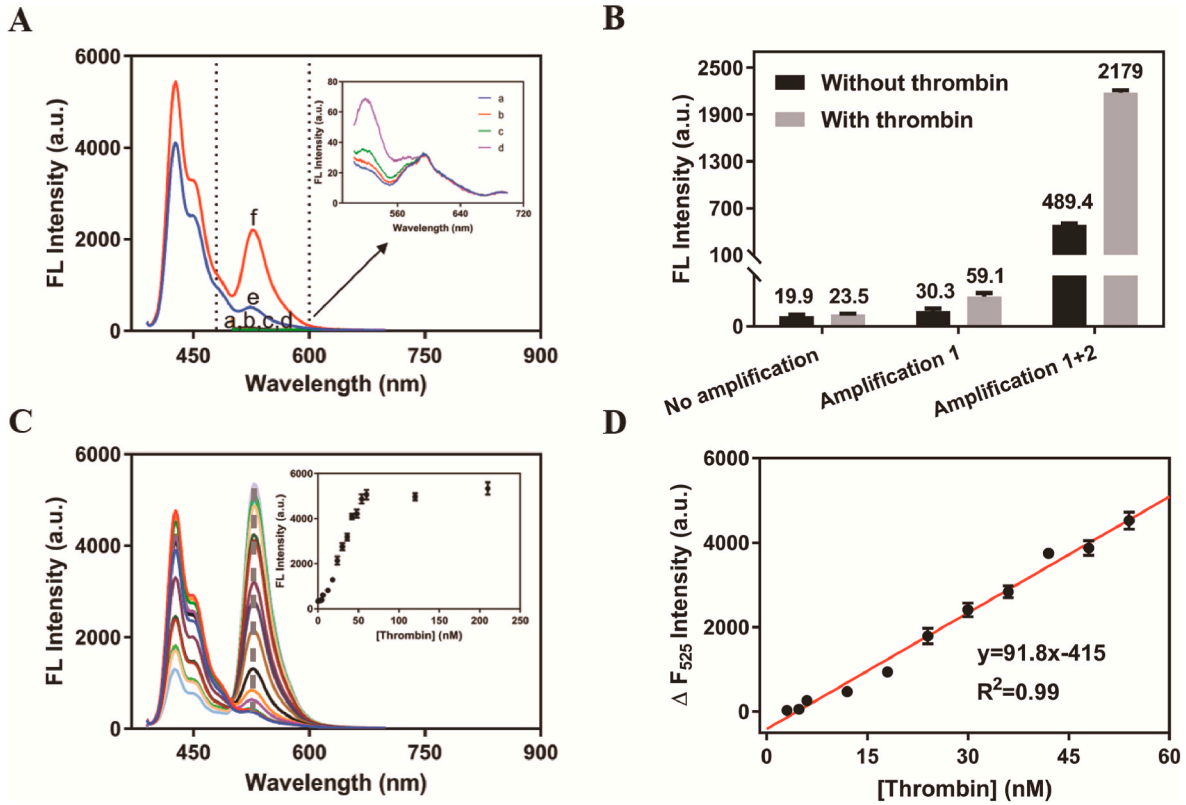

Fig. 3. (A) Fluorescence emission spectra of the dual amplification protein detection system under different conditions. Curve a: HT1+GO; Curve b: HT1+Thrombin+GO; Curve c: HT1+HT2+GO; Curve d: HT1+HT2+Thrombin+GO; Curve e: HT1+HT2+GO+PFP; Curve f: HT1+HT2+Thrombin+GO+PFP. (B) Histogram of the change of fluorescence intensity with or without thrombin under different conditions. The fluorescence intensities were recorded at 520 nm for No amplification based on the curve a and b in Fig. 3A and Amplification 1 based on the curve c and d in Fig. 3A. The fluorescence intensities were recorded at 525 nm for Amplification 1 + 2 based on the curve e and f in Fig. 3A. (C) Fluorescence responses to the different concentrations of the thrombin with CHA and PFP dual amplification. The grey dash line shows the peak of FAM signal at 525 nm. The insert shows the fluorescence intensity at 525 nm to different concentrations of the thrombin. (D) The linear fitting curve of ΔF_{525} and the thrombin concentration with CHA and PFP dual amplification. Error bars represent the standard deviation of three measurements.

The aptamer sequence of the thrombin was designed in the loop and stem part of the hairpin HT1 (orange line in HT1). In the presence of the thrombin, the conjugate of the thrombin and its aptamer will change the secondary structure of HT1 and release the toehold region (blue line in HT1). This toehold area will open the hairpin HT2, lead to form the HT1-HT2 dsDNA complex, and dissociate the thrombin from HT1. The thrombin then could continue to bind with another HT1 and repeat the above process. Finally, the whole system will accumulate numerous HT1-HT2 complex. As in the strategy for DNA detection, the HT1-HT2 complex could depart from the surface of GO and bind with PFP to give out a FRET signal from PFP to FAM-labeled on HT1 and HT2.

The feasibility of this design was verified by recording fluorescence spectra in the response of the thrombin detection under different conditions shown in Fig. 3A. Without the aid of CHA or PFP (No amplification in Fig. 3B), the thrombin produced limited fluorescence signal and the fluorescence intensity at 520 nm changed just from 19.1 (without thrombin) to 23.5 (with thrombin) according to curve a and b in Fig. 3A (ex: 480 nm). In CHA assisted amplification (Amplification 1 in Fig. 3B), the fluorescence signal at 520 nm changed from 29.3 (without thrombin) to 60.0 (with thrombin) according to curve c and d in Fig. 3A (ex: 480 nm). Upon the addition of PFP in the CHA system, the fluorescence intensity at 525 nm enhanced drastically (curve e and f in Fig. 3A, ex: 370 nm). And the fluorescence recovery with thrombin reached 1600 (Amplification 1 + 2 in Fig. 3B). Thus, the dual amplification strategy also works for thrombin detection.

Then, the reaction conditions, including the concentrations of GO and PFP, were optimized. As shown in Fig. S5, we chose to use 1.33 μg mL^{-1} of GO and 1.33 μg mL^{-1} of PFP to obtain the best signal to noise ratio for further experiment. Under the optimized conditions, the sensitivity for thrombin detection was evaluated with different concentrations of the thrombin. As shown in Fig. 3C, fluorescence intensity at 525 nm raised as the thrombin concentration increased. In the range from 3 to 54 nM of the thrombin, the fluorescence recovery at 525 nm (ΔF_{525}) and the thrombin concentration showed a good linear relationship. The linear regression equation can be expressed with $y = 91.8x\text{-}415$ ($R^2 = 0.99$, RSD ranged from 3.3% to 10.4%), where y represents the fluorescence intensity difference of with or without thrombin and x is the thrombin concentration. The LOD was estimated to be 11 pM based on the calculation method of 3σ/k and the LOQ was calculated to be 33 pM according to the 10σ/k. Compared with other enzyme-free methods for thrombin detection, our strategy shows comparable analysis performance while our approach has the advantage of simplicity and universality (Table S3). Furthermore, several other interferents (IgG, trypsin, pepsin, BSA, β-dextranse, mucoprotein and lecithin) were selected to explore the selectivity of our method. As shown in Fig. S6, only the thrombin generated a significant fluorescence enhancement, which suggested the excellent selectivity of this assay. We also tested the potential of this method for real sample detection by the recovery assay [39,40]. 5, 10, and 20 nM thrombin was used to conduct the recovery test. And the recovery was calculated with a range of 94.7–103.7% (Table S4), which indicated this method could be used in biological samples with a satisfactory anti-interference ability.

4. Conclusions

A CHA/CCP/GO-assisted dual amplification strategy was proposed for simple, sensitive, selective, and enzyme-free DNA and thrombin detection. This assay offers several advantages. Firstly, taking advantage of the cation conjugated polymer PFP, dsDNA product from CHA can be further amplified with simple amplification procedure and short reaction time. Secondly, GO was used to reduce the background due to its high absorption ability and quenching efficiency to FAM-labeled hairpin DNA. Thirdly, CHA and PFP dual amplification avoids the use of enzymes and offers excellent amplification efficiency.

Moreover, various molecules can be detected by simply changing the sequences of hairpin DNA. Besides the DNA targets, proteins or small molecules with suitable aptamers such as thrombin, the transmembrane glycoprotein mucin 1 (MUC1), adenosine triphosphate (ATP), zearalenone and tetracycline can be potentially determined using this biosensor [41–44]. This strategy also reveals good performance in 1% human serum and shows little interference for real sample detection. Still, there are some limitations to our strategy. Firstly, simultaneous detection of multiple targets in one tube is limited by the single FRET fluorescence signal output in our strategy. Secondly, potential analytes are limited by the number of aptamers.

Credit author statement

Zhen Zhang: Conceptualization, Methodology, Investigation, Writing - original draft, Xia Xiang: Conceptualization, Investigation Yuqiang Hu: Investigation Yuhan Deng: Writing - review & editing, Longjie Li: Investigation Wenbo Zhao: Conceptualization, Writing - review & editing, Tongbo Wu: Supervision, Funding acquisition, Writing - review & editing.

Declaration of competing interest

The authors declare that they have no known competing financial interests or personal relationships that could have appeared to influence the work reported in this paper.

Acknowledgements

This work was supported by the National Natural Science Foundation of China (No. 21904045) and the Fundamental Research Funds for the Central Universities (HUST: No. 2019kfyXJJS169).

Appendix A. Supplementary data

Supplementary data to this article can be found online at https://doi.org/10.1016/j.talanta.2020.121716.

References

[1] H. Zhang, F. Li, B. Dever, X.F. Li, X.C. Le, DNA-mediated homogeneous binding assays for nucleic acids and proteins, Chem. Rev. 113 (4) (2013) 2812–2841.
[2] L. Cohen, D.R. Walt, Highly sensitive and multiplexed protein measurements, Chem. Rev. 119 (1) (2019) 293–321.
[3] Y. Du, S. Dong, Nucleic acid biosensors: recent advances and perspectives, Anal. Chem. 89 (1) (2017) 189–215.
[4] N. Chen, X. Ouyang, M. Lin, N. Liu, T. Wu, X. Xiao, Branch migration based selective PCR for DNA mutation enrichment and detection, Chem. Commun. 55 (58) (2019) 8466–8469.
[5] L. Becherer, N. Borst, M. Bakheit, S. Frischmann, R. Zengerle, F. von Stetten, Loop-mediated isothermal amplification (LAMP) – review and classification of methods for sequence-specific detection, Anal. Methods 12 (6) (2020) 717–746.
[6] F. Ma, H. Liu, C.C. Li, C.Y. Zhang, A simple and isothermal ligase-based amplification approach based on a ligation-activated cleavage reaction, Chem. Commun. 54 (89) (2018) 12638–12641.
[7] L. Zhang, Y. Zhang, L. Huang, Y. Zhang, Y. Li, S. Ding, W. Cheng, Ultrasensitive biosensing of low abundance BRAF V600E mutation in real samples by coupling dual padlock-gap-ligase chain reaction with hyperbranched rolling circle amplification, Sensor. Actuator. B Chem. 287 (2019) 111–117.
[8] Q. Feng, L. Qin, M. Wang, P. Wang, Signal-on electrochemical detection of DNA methylation based on the target-induced conformational change of a DNA probe and exonuclease III-assisted target recycling, Biosens. Bioelectron. 149 (2020) 111847.
[9] X. Xiao, Y. Liu, M. Zhao, Endonuclease IV discriminates mismatches next to the apurinic/apyrimidinic site in DNA strands: constructing DNA sensing platforms with extremely high selectivity, Chem. Commun. 49 (27) (2013) 2819–2821.
[10] Z. Ning, Y. Zheng, D. Pan, Y. Zhang, Y. Shen, Coupling aptazyme and catalytic hairpin assembly for cascaded dual signal amplified electrochemiluminescence biosensing, Biosens. Bioelectron. 150 (2020) 111945.
[11] J. Liu, Y. Zhang, H. Xie, L. Zhao, L. Zheng, H. Ye, Applications of catalytic hairpin assembly reaction in biosensing, Small 15 (2019) 1902989.
[12] Z. Zhang, Y. Liu, X. Ji, X. Xiang, Z. He, A graphene oxide-based enzyme-free signal amplification platform for homogeneous DNA detection, Analyst 139 (19) (2014) 4806–4809.
[13] H. Li, J. Ren, Y. Liu, E. Wang, Application of DNA machine in amplified DNA detection, Chem. Commun. 50 (6) (2014) 704–706.
[14] Y. Zhang, S. Luo, B. Situ, Z. Chai, B. Li, J. Liu, L. Zheng, A novel electrochemical cytosensor for selective and highly sensitive detection of cancer cells using binding-induced dual catalytic hairpin assembly, Biosens. Bioelectron. 102 (2018) 568–573.
[15] X. Liu, X. Zhou, X. Xia, H. Xiang, Catalytic hairpin assembly-based double-end DNAzyme cascade-feedback amplification for sensitive fluorescence detection of HIV-1 DNA, Anal. Chim. Acta 1096 (2020) 159–165.
[16] G. Dong, J. Dai, L. Jin, H. Shi, F. Wang, C. Zhou, B. Zheng, Y. Guo, D. Xiao, A rapid room-temperature DNA amplification and detection strategy based on nicking endonuclease and catalyzed hairpin assembly, Anal. Methods 11 (19) (2019) 2537–2541.
[17] C. Park, Y. Song, K. Jang, C.-H. Choi, S. Na, Target switching catalytic hairpin assembly and gold nanoparticle colorimetric for EGFR mutant detection, Sensor. Actuator. B Chem. 261 (2018) 497–504.
[18] T. Ye, Y. Peng, M. Yuan, H. Cao, J. Yu, Y. Li, F. Xu, Target-induced in-situ formation of fluorescent DNA-templated copper nanoparticles by a catalytic hairpin assembly: application to the determination of DNA and thrombin, Microchim. Acta 186 (12) (2019) 760.
[19] X. Duan, L. Liu, F. Feng, S. Wang, Cationic conjugated polymers for optical detection of DNA methylation, lesions, and single nucleotide polymorphisms, Acc. Chem. Res. 43 (2) (2010) 260–270.
[20] C. Zhu, L. Liu, Q. Yang, F. Lv, S. Wang, Water-soluble conjugated polymers for imaging, diagnosis, and therapy, Chem. Rev. 112 (8) (2012) 4687–4735.
[21] Y. Zhou, J. Zhang, L. Zhao, Y. Li, H. Chen, S. Li, Y. Cheng, Visual detection of multiplex MicroRNAs using cationic conjugated polymer materials, ACS Appl. Mater. Interfaces 8 (2) (2016) 1520–1526.
[22] M. Liu, B. Li, Detection of DNA hybridization using a cationic polyfluorene polymer as an enhancer of luminol chemiluminescence, Mikrochim. Acta 183 (2) (2016) 897–903.
[23] F. Feng, L. Liu, S. Wang, Fluorescent conjugated polymer-based FRET technique for detection of DNA methylation of cancer cells, Nat. Protoc. 5 (7) (2010) 1255–1264.
[24] Z. Zhang, X. Xia, X. Xiang, F. Huang, L. Han, Conjugated cationic polymer-assisted amplified fluorescent biosensor for protein detection via terminal protection of small molecule-linked DNA and graphene oxide, Sensor. Actuator. B Chem. 249 (2017) 8–13.
[25] V. Georgakilas, J.N. Tiwari, K.C. Kemp, J.A. Perman, A.B. Bourlinos, K.S. Kim, R. Zboril, Noncovalent functionalization of graphene and graphene oxide for energy materials, biosensing, catalytic, and biomedical applications, Chem. Rev. 116 (9) (2016) 5464–5519.
[26] J. Lin, X. Chen, P. Huang, Graphene-based nanomaterials for bioimaging, Adv. Drug Deliv. Rev. 105 (2016) 242–254.
[27] P. Bollella, G. Fusco, C. Tortolini, G. Sanzò, G. Favero, L. Gorton, R. Antiochia, Beyond graphene: electrochemical sensors and biosensors for biomarkers detection, Biosens. Bioelectron. 89 (2017) 152–166.
[28] H. Zhang, H. Zhang, A. Aldalbahi, X. Zuo, C. Fan, X. Mi, Fluorescent biosensors enabled by graphene and graphene oxide, Biosens. Bioelectron. 89 (2017) 96–106.
[29] Z. Huang, Z. Luo, J. Chen, Y. Xu, Y. Duan, A facile, label-free, and universal biosensor platform based on target-induced graphene oxide constrained DNA dissociation coupling with improved strand displacement amplification, ACS Sens. 3 (11) (2018) 2423–2431.
[30] X.J. Xing, X.G. Liu, Y. He, Y. Lin, C.L. Zhang, H.W. Tang, D.W. Pang, Amplified fluorescent sensing of DNA using graphene oxide and a conjugated cationic polymer, Biomacromolecules 14 (1) (2013) 117–123.
[31] Z. Zhang, X. Xiang, J. Shi, F. Huang, X. Xia, M. Zheng, L. Han, H. Tang, A cationic conjugated polymer and graphene oxide: application to amplified fluorescence detection of sinapine, Spectrochim. Acta Mol. Biomol. Spectrosc. 203 (2018) 370–374.
[32] R. Pautler, E.Y. Kelly, P.J.J. Huang, J. Cao, B. Liu, J. Liu, Attaching DNA to nanoceria: regulating oxidase activity and fluorescence quenching, ACS Appl. Mater. Interfaces 5 (15) (2013) 6820–6825.
[33] G.H. Chen, W.Y. Chen, Y.C. Yen, C.W. Wang, H.T. Chang, C.F. Chen, Detection of mercury(II) ions using colorimetric gold nanoparticles on paper-based analytical devices, Anal. Chem. 86 (14) (2014) 6843–6849.
[34] L. Lan, D. Chen, Y. Yao, X. Peng, J. Wu, Y. Li, J. Ping, Y. Ying, Phase-dependent fluorescence quenching efficiency of MoS2 nanosheets and their applications in multiplex target biosensing, ACS Appl. Mater. Interfaces 10 (49) (2018) 42009–42017.

[35] S. Zhang, K.B. Li, Y. Pan, D.M. Han, Ultrasensitive detection of ochratoxin A based on biomimetic nanochannel and catalytic hairpin assembly signal amplification, Talanta 220 (2020) 121420.
[36] B. Deng, Y. Lin, C. Wang, F. Li, Z. Wang, H. Zhang, X.F. Li, X.C. Le, Aptamer binding assays for proteins: the thrombin example—a review, Anal. Chim. Acta 837 (2014) 1–15.
[37] D.M. Tasset, M.F. Kubik, W. Steiner, Oligonucleotide inhibitors of human thrombin that bind distinct epitopes11Edited by R, Huber, JMB 272 (5) (1997) 688–698.
[38] Y. Fan, F. Liao, W. Wu, N. Hong, L. Cheng, Y. Zhong, H. Cui, G. Ma, G. Wei, J. Xiong, H. Fan, A novel modification-free thrombin electrochemical sensing based homogeneous strategy, Sensor. Actuator. B Chem. 318 (2020) 128045.
[39] M. Stafiński, M. Wieczorek, P. Janicki, P. Kościelniak, Theoretical and experimental examination of recovery in the context of trueness of analytical results, Talanta 96 (2012) 39–43.
[40] M. Stafiński, M. Wieczorek, P. Kościelniak, Influence of the species effect on trueness of analytical results estimated by the recovery test when determining selenium by HG-AFS, Talanta 117 (2013) 64–69.
[41] J. Li, J. Liu, Y. Bi, M. Sun, J. Bai, M. Zhou, Ultrasensitive electrochemiluminescence biosensing platform for miRNA-21 and MUC1 detection based on dual catalytic hairpin assembly, Anal. Chim. Acta 1105 (2020) 87–94.
[42] Z. Tian, P. Peng, H. Wang, J. Zheng, L. Shi, T. Li, Aptamer-braked multi-hairpin cascade circuits for logic-controlled label-free in situ bioimaging, Anal. Chem. 92 (15) (2020) 10357–10364.
[43] N. Yin, S. Yuan, M. Zhang, J. Wang, Y. Li, Y. Peng, J. Bai, B. Ning, J. Liang, Z. Gao, An aptamer-based fluorometric zearalenone assay using a lighting-up silver nanocluster probe and catalyzed by a hairpin assembly, Microchim Acta 186 (12) (2019) 765.
[44] Y. Wang, L. Yao, G. Ning, Y. Wu, S. Wu, S. Mao, G.Q. Liu, An electrochemical strategy for tetracycline detection coupled triple helix aptamer probe with catalyzed hairpin assembly signal amplification, Biosens. Bioelectron. 143 (2019) 111613.